Optimal and Direct-Current Vector Control of Direct-Driven PMSG Wind Turbines

Shuhui Li, *Senior Member, IEEE*, Timothy A. Haskew, *Senior Member, IEEE*, Richard P. Swatloski, and William Gathings

***Abstract*—With the advances of power electronic technology, direct-driven permanent magnet synchronous generators (PMSGs) have increasingly drawn the interest of wind turbine manufacturers. At the present time, a commercial PMSG wind turbine primarily makes use of a passive rectifier followed by an insulated gate bipolar transistor (IGBT) inverter. Although a PMSG wind turbine with two back-to-back voltage source IGBT converters is considered more efficient, it has not been widely adopted by the wind power industry. This paper investigates both the conventional and a novel vector control mechanism for a PMSG wind turbine that has two side-by-side voltage source pulsewidth modulation converters. The proposed approach is based on a direct-current vector control mechanism for control of both machine- and grid-side converters of a PMSG wind turbine. Then, an optimal control strategy is developed for integrated control of PMSG maximum power extraction, reactive power, and grid voltage support controls. A transient system simulation using SimPowerSystem is built to investigate the performance of the conventional and proposed control techniques for the PMSG wind turbine under steady and gusty wind conditions. This paper shows that when using the direct-current vector control structure, a PMSG system has excellent performance in various aspects.**

***Index Terms*—DC-link voltage control, direct-current vector control, grid voltage support control, maximum wind power extraction, optimal control, permanent magnet synchronous generator (PMSG) wind turbine, reactive power control, voltage source converter (VSC).**

I. Introduction

WIND power is today's most rapidly growing renewable energy source. A wind turbine operates either at a fixed or variable speed [1]. Most of the major wind turbine manufacturers are developing new megawatt scale wind turbines based on variable-speed operation with pitch control using either a permanent magnet synchronous generator (PMSG) or a doubly fed induction generator (DFIG) [2].

The variable speed wind turbine with a multipole PMSG and full-scale/fully controllable voltage source converters (VSCs) is considered to be a promising, but not yet very popular, wind turbine concept [3]. The advantages of such a PMSG configuration are 1) gearless construction [4]; 2) the elimination of a dc excitation system [5]; 3) full controllability of the system for maximum wind power extraction and grid interface; and 4) ease in accomplishing fault-ride through and grid support [6]. Therefore, the efficiency and reliability of a VSC-based PMSG wind turbine is assessed to be higher than that of a DFIG wind turbine [7]. Due to the intensified grid codes, a PMSG wind turbine with full VSC-based insulated gate bipolar transistor (IGBT) converters is becoming more and more favored by the wind power industry [3]–[7].

At the present time, however, commercial PMSG technology mainly uses a passive rectifier followed by an IGBT inverter [8]–[11]. The highly efficient vector-controlled technology for a PMSG wind turbine that uses a full voltage-source IGBT converter configuration is still under investigation [12]–[14] and not widely adopted by the wind power industry. The direct-current vector control technology is a vector control technology that has been developed recently for control of the synchronous generator only in a variable-speed PMSG wind turbine [15], [16] and for control of a VSC-based HVDC system [17]. Compared to the conventional vector control strategies, direct-current vector control has demonstrated many advantages in those applications, such as enhanced system stability, reliability, and efficiency. But it is not clear whether the direct-current vector control can be employed in a PMSG wind turbine for control of both PMSG machine- and grid-side converters (GSCs), and how the PMSG system will behave in the integrated environment for multiple PMSG control purposes.

This paper presents mechanisms for optimal control of a PMSG wind turbine system under a direct-current *dq* vector control configuration. Then, based on the proposed control structure, the overall control functions of a PMSG system are developed, including maximum power extraction control, dc-link voltage control, reactive power control, and grid voltage support control. The proposed control mechanism is compared with the conventional vector control method. In the sections that follow, this paper first introduces the general configuration of a PMSG system and overall control functions in Section II. Then, Section III presents the conventional and direct-current vector control design for the PMSG machine-side converter (MSC). The conventional and direct-current vector control design of the GSC is given in Section IV. Section V shows the control integration of the MSC and GSC for PMSG maximum wind power extraction, reactive power, and grid voltage support controls. Simulation studies are conducted in Section VI to examine

Manuscript received April 16, 2011; revised July 13, 2011; accepted October 15, 2011. Date of current version February 27, 2012. Recommended for publication by Associate Editor Z. Chen.

S. Li and T. A. Haskew are with the Department of Electrical and Computer Engineering, The University of Alabama, Tuscaloosa, AL 35487 USA (e-mail: sli@eng.ua.edu; thaskew@eng.ua.edu).

R. P. Swatloski and W. Gathings are with the Office for Technology Transfer, The University of Alabama, Tuscaloosa, AL 35487 USA (e-mail: richard.swatloski@ua.edu; william.gathings@ua.edu).

Color versions of one or more of the figures in this paper are available online at http://ieeexplore.ieee.org.

Digital Object Identifier 10.1109/TPEL.2011.2174254

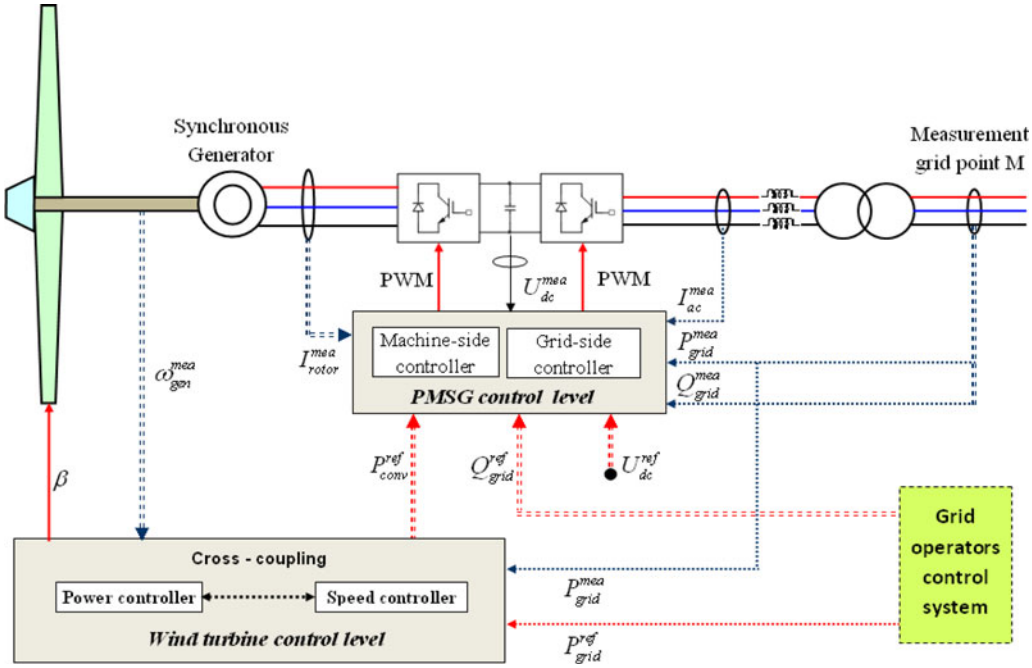

Fig. 1. Configuration of a PMSG wind turbine.

and compare the performance of the proposed and conventional control strategies under steady and variable wind conditions. Finally, the paper concludes with the summary of the main points.

II. PMSG Mechanical/Electrical Systems and Integrated Controls

A VSC-based PMSG wind turbine consists mainly of three parts: a wind turbine drive train, a PMSG, and two back-to-back VSCs (see Fig. 1) [12]. In the turbine drive train, the rotor blades of the wind turbine catch wind energy that is then transferred to the generator. The generator, converting mechanical energy into electrical energy, is a standard permanent magnet synchronous machine with its stator windings connected to the grid through a frequency converter. The frequency converter is built by two current-regulated voltage-source pulsewidth modulation (PWM) converters: an MSC and a GSC, with a dc voltage link in between [12], [13], [18].

The control of the PMSG system has three levels: the generator level, the wind turbine level, and the wind power plant level (see Fig. 1) [12], [19]. At the generator level, each of the two VSCs (see Fig. 1) is controlled through decoupled *dq* vector control approaches in the conventional technology. The MSC controls the PMSG to achieve the following goals: maximum energy extraction from the wind and/or compliance with a control demand from the wind power plant control center. The GSC maintains a constant dc-link voltage and adjusts reactive power absorbed from the grid by the converter. At the wind turbine level, there is a speed controller and a power limiting controller. At low wind speeds, the speed controller gives a power or torque reference to the MSC controller based on the principle of maximum energy capture. The power limiting controller increases or decreases the pitch angle of wind turbine blades to prevent the turbine from going over the rated power at high wind speeds. At the wind power plant level, the power production of the entire plant is determined based on the grid requirements. The central control system sends out reference power signals to each individual wind turbine according to a grid need, while the local turbine control system ensures that the reference power signal sent by the central control system is reached [19].

III. Conventional and Direct-Current Vector Control of MSC

A. Generator Model

A commonly used PMSG transient model is the Park model. Using generator convention, space vector theory yields the stator voltage equation in the form [20]

$$\begin{pmatrix} v_{sd} \\ v_{sq} \end{pmatrix} = -R_s \begin{pmatrix} i_{sd} \\ i_{sq} \end{pmatrix} - \frac{d}{dt} \begin{pmatrix} \psi_{sd} \\ \psi_{sq} \end{pmatrix} + \omega_e \begin{pmatrix} 0 & -1 \\ 1 & 0 \end{pmatrix} \begin{pmatrix} \psi_{sd} \\ \psi_{sq} \end{pmatrix} \tag{1}$$

where R_s is the resistance of the stator winding, ω_e is the generator electrical rotational speed, and v_{sd}, v_{sq}, i_{sd}, i_{sq} ψ_{sd}, and ψ_{sq} are the *d*- and *q*-component of instant stator voltage, current, and flux. If the *d*-axis is aligned along the rotor flux position, the stator flux linkages are

$$\begin{pmatrix} \psi_{sd} \\ \psi_{sq} \end{pmatrix} = \begin{pmatrix} L_{ls} + L_{dm} & 0 \\ 0 & L_{ls} + L_{qm} \end{pmatrix} \begin{pmatrix} i_{sd} \\ i_{sq} \end{pmatrix} + \begin{pmatrix} \psi_f \\ 0 \end{pmatrix} \tag{2}$$

where L_{ls} is the leakage inductance of the stator winding, L_{dm} and L_{qm} are the stator and rotor *d*- and *q*-axis mutual inductances, respectively, ψ_f is the flux linkage produced by the permanent magnet. The electromagnetic torque is

$$\tau_{\mathrm{em}} = p\left(\psi_{sd} i_{sq} - \psi_{sq} i_{sd}\right) = p\left(\psi_f i_{sq} + \left(L_d - L_q\right) i_{sd} i_{sq}\right) \tag{3}$$

where $L_d = L_{ls} + L_{dm}$ and $L_q = L_{ls} + L_{qm}$. Under the steady-state condition, (1) reduces to

$$\begin{pmatrix} V_{sd} \\ V_{sq} \end{pmatrix} = \begin{pmatrix} -R_s & -\omega_e L_q \\ \omega_e L_d & -R_s \end{pmatrix} \begin{pmatrix} I_{sd} \\ I_{sq} \end{pmatrix} + \begin{pmatrix} 0 \\ \omega_e \psi_f \end{pmatrix}. \quad (4)$$

Normally, the difference between the d- and q-axis mutual inductance is very small for a direct-driven multipole PMSG [21], [22], and the stator winding resistance is much smaller than the synchronous reactance. Therefore, (3) reduces to (5), and the steady-state stator d- and q-axis currents obtained from (4) are given by

$$\tau_{\rm em} = p\psi_f i_{sq} \quad (5)$$

$$I_{sq} = -V_{sd}/(\omega_e L_q), I_{sd} = (V_{sq} - \omega_e \psi_f)/(\omega_e L_d). \quad (6)$$

B. Wind Turbine Model

The mechanical power extracted by a wind turbine from the wind is expressed by the cube law equation [23]

$$P_w = \frac{1}{2}\rho_{\rm air} A_{\rm blade} C_p(\beta, \lambda) \cdot v_w^3 \quad (7)$$

$$\lambda = R_{\rm blade}\omega_m / v_w \quad (8)$$

where $\rho_{\rm air}$ is the air density, $A_{\rm blade}$ is the area covered by the rotor blades, C_p is the turbine performance coefficient, v_w is the wind speed, $R_{\rm blade}$ is the radius of the rotor blades, and ω_m is the wind turbine rotor rotational speed. The performance coefficient C_p is a function of the tip-speed-ratio λ (8) and the pitch angle β of the rotor blades [24]. For a given wind speed and pitch angle, there is an optimal tip-speed-ratio $\lambda_{\rm opt}$ and an optimal turbine rotating speed $\omega_{m\_\rm opt}$ under which C_p takes a maximum value, i.e., maximum power extraction from the wind for that pitch angle

$$\omega_e = p \cdot \omega_g, \omega_g = n_{\rm gear} \cdot \omega_m. \quad (9)$$

The relation among ω_m, ω_g (generator rotational speed), and ω_e is presented in (9), where p is the generator pole pairs. For a direct-driven PMSG system, $n_{\rm gear} = 1$. Using generator convention, the rotational speed of the generator and wind turbine driving torque follows from

$$\tau_w = J_{\rm eq}\frac{d\omega_g}{dt} + B_a\omega_g + \tau_{\rm em} \quad (10)$$

where τ_w is the turbine driving torque referred to the generator, $J_{\rm eq}$ is the total equivalent inertia referred to the generator, and B_a is the active damping coefficient representing turbine rotational losses.

C. Conventional Vector Control of MSC

The conventional vector control method for the MSC has a nested-loop structure consisting of a faster inner current loop and a slower outer loop as shown by Fig. 2 [12], in which the q-axis loop is for wind turbine speed or torque control and the d-axis loop is for other control purposes. The control strategy of the inner current loop is developed by rewriting (1) and (2) as

$$v_{sd} = -\left(R_s i_{sd} + L_d\frac{di_{sd}}{dt}\right) - \omega_e L_q i_{sq} \quad (11)$$

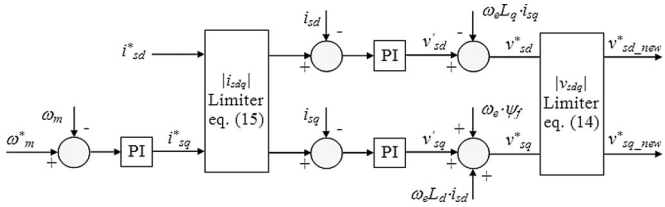

Fig. 2. Conventional MSC vector control structure.

$$v_{sq} = -\left(R_s i_{sq} + L_q\frac{di_{sq}}{dt}\right) + \omega_e L_d i_{sd} + \omega_e \psi_f \quad (12)$$

where the item in the bracket of (11) and (12) is treated as the state equation between the voltage and current in the d- and q-loop, and the other items are treated as compensation terms [12], [25]. This treatment assumes that v_{sd} in (11) has no major influence on i_{sq} and that v_{sq} in (12) has no significant effect on i_{sd}.

But this assumption is inadequate as explained as follows. According to Fig. 2, the final control voltages v^*_{sd} and v^*_{sq}, linearly proportional to the converter output voltages V_{sd} and V_{sq} [25], include the d- and q-axis voltages v'_{sd} and v'_{sq} generated by the current-loop controllers plus the compensation terms as shown by (13). Hence, the conventional control configuration intends to regulate i_{sd} and i_{sq} using v'_{sd} and v'_{sq}, respectively. But, according to (5) and (6), the d-axis voltage is only effective for i_{sq} or torque control, and the q-axis voltage is only effective for i_{sd} control

$$v^*_{sd} = v'_{sd} - \omega_e L_q i_{sq}, v^*_{sq} = v'_{sq} + \omega_e L_d i_{sd} + \omega_e \psi_f. \quad (13)$$

The following issues are considered in the design of the conventional nested-loop control system.

1) To prevent the MSC from getting into the nonlinear modulation mode, a saturation mechanism is applied if the amplitude of the reference voltage generated by the inner current-loop controller exceeds the converter linear modulation limit. The general strategy is to set a limitation on $\left|v^*_{sdq}\right|$ but keep $\angle v^*_{sdq}$ unchanged as shown by (14) [26], where $v^*_{sd\_\rm new}$ and $v^*_{sq\_\rm new}$ are the d- and q-component of the modified controller output voltage, and $V_{\rm max\_MSC}$ is the maximum allowable dq voltage. It is found that any other saturation mechanisms could cause more system oscillation and unbalance

$$v^*_{sd\_\rm new} = V_{\rm max\_MSC}\cos\left(\angle v^*_{sdq}\right)$$
$$v^*_{sq\_\rm new} = V_{\rm max\_MSC}\sin\left(\angle v^*_{sdq}\right). \quad (14)$$

2) To prevent the MSC or the generator from exceeding the rated current, the d-axis current reference is adjusted if the amplitude of the reference current generated by the outer control loop exceeds the rated current limit. The general approach is keeping the q-axis current reference i^*_{sq} unchanged to maintain wind turbine control effectiveness while modifying the d-axis current reference i^*_{sd} to satisfy the d-axis control demand as much as possible as shown

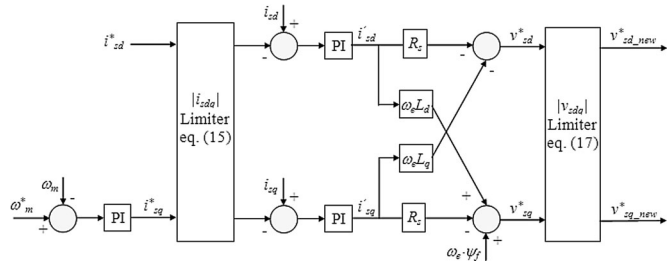

Fig. 3. Direct-current vector control structure of the MSC.

by (15) [26]

$$i^*_{sd\_\text{new}} = \text{sign}\left(i^*_{sd}\right)\cdot\sqrt{\left(i^*_{sdq\_\max}\right)^2 - \left(i^*_{sq}\right)^2}$$
$$i^*_{sq\_\text{new}} = i^*_{sq}. \tag{15}$$

D. Direct-Current Vector Control of MSC

The direct-current vector control strategy of the MSC, implemented also through a nested-loop control structure (see Fig. 3), includes the following three parts: 1) transformation from speed control to current control; 2) development of a direct-current control mechanism; and 3) conversion from current control signals to voltage control signals.

First, the transformation from speed to torque control is accomplished through a speed-loop controller that is designed based on (10). Then, the torque control is converted to stator q-axis current control, according to (5), while the stator d-axis current is set to zero (i.e., a minimum stator current control strategy).

Second, the d- and q-axis currents generated by the speed-loop controller are used as reference signals to an inner current-loop controller. It is necessary to point out that a fast current-loop controller is crucial to assure high-performance operation of the synchronous generator in terms of reduced harmonics and stator current unbalance. Although direct power control strategies have been proposed recently for control of DFIG wind turbines [27], [28], many disadvantages, such as poor power quality, have been found due to the elimination of the current control loop [29], [30]. However, unlike the conventional vector control strategy that outputs a d- or q-axis voltage based on a d- or q-axis current error signal (see Fig. 2), the direct-current vector control mechanism of the MSC outputs d- and q-axis tuning currents i'_{sd} and i'_{sq}, in which the input error signal tells the controller how much the tuning current should be adjusted through an adaptive tuning strategy [31]–[33].

Third, due to a VSC structure of the MSC, the stator d- and q-axis tuning current signals i'_{sd} and i'_{sq} generated by the current-loop controllers are transferred to stator d- and q-axis voltage signals v^*_{sd} and v^*_{sq} to control the synchronous generator. The conversion from the current to voltage control signals is implemented through (16), which is equivalent to the transient dq (1) after being processed by a low-pass filter to reduce the oscillation of d- and q-axis reference voltages applied directly to the converter

$$v^*_{sd} = -R_s i'_{sd} - \omega_e L_q i'_{sq}$$
$$v^*_{sq} = -R_s i'_{sq} + \omega_e L_d i'_{sd} + \omega_e \psi_f. \tag{16}$$

Signal processing technology is applied to the measured d- and q-axis currents in Fig. 3 to prevent the higher order harmonics of the d- and q-axis currents from entering the controllers. In addition, a nonlinear programming formulation, as shown in the following, is developed to minimize the error between the actual and desired d-axis current while preventing the resultant dq current from exceeding the rated current and preventing the converter from entering the nonlinear modulation mode [34]. The constraints of the nonlinear programming formulation force the q-axis current to the desired value, limit the MSC phase rms current to $I_{\text{MSC\_rated}}$, and maintain linear modulation constraints.

Minimize: $|i_{sd} - i^*_{sd}|$

Subject to: $i_{sq} = i^*_{sq}$

$$\sqrt{\frac{i^2_{sd} + i^2_{sq}}{3}} \le I_{\text{MSC\_rated}}, \quad \sqrt{\frac{v^2_{sd} + v^2_{sq}}{3}} \le \frac{V_{\text{dc}}}{2\sqrt{2}}.$$

The nonlinear programming strategy is implemented in the following way. If $|i^*_{sdq}|$ generated by the outer control loop exceeds the rated current limit, i^*_{sd} and i^*_{sq} are modified by (15). If $|v^*_{sdq}|$ generated by the current control loops exceeds the PWM saturation limit, v^*_{sd} and v^*_{sq} are modified by (17). According to (5) and (6), (17) represents an optimal strategy for keeping the d-axis voltage reference v^*_{sd} unchanged so as to maintain the wind turbine speed control effectiveness while modifying the q-axis voltage reference v^*_{sq} to meet the d-axis control demand as much as possible. But (17) cannot be applied to the conventional control structure (see Fig. 2); that could result in major oscillation and unbalance problems due to the competing control nature of the conventional dq control method

$$v^*_{sd\_\text{new}} = v^*_{sd}$$
$$v^*_{sq\_\text{new}} = \text{sign}\left(v^*_{sq}\right)\cdot\sqrt{\left(v^*_{sdq\_\max}\right)^2 - \left(v^*_{sd}\right)^2}. \tag{17}$$

IV. Conventional and Direct-Current Vector Control of GSC

A. GSC Model

Fig. 4 shows the schematic of the GSC, in which the dc-link capacitor is on the left and a three-phase voltage source, representing the voltage at the point of common coupling (PCC) of the ac system, is on the right. In the dq reference frame, the voltage balance across the grid filter is

$$\begin{bmatrix} v_{d1} \\ v_{q1} \end{bmatrix} = R_f \begin{bmatrix} i_d \\ i_q \end{bmatrix} + L_f \frac{d}{dt}\begin{bmatrix} i_d \\ i_q \end{bmatrix} + \omega_s L_f \begin{bmatrix} -i_q \\ i_d \end{bmatrix} + \begin{bmatrix} v_d \\ v_q \end{bmatrix} \tag{18}$$

where ω_s is the angular frequency of the grid voltage, L_f and R_f are the inductance and resistance of the grid filter, respectively, v_d, v_q, v_{d1}, and v_{q1} represent the d- and q-axis components of the PCC voltage and GSC output voltage, respectively, and i_d

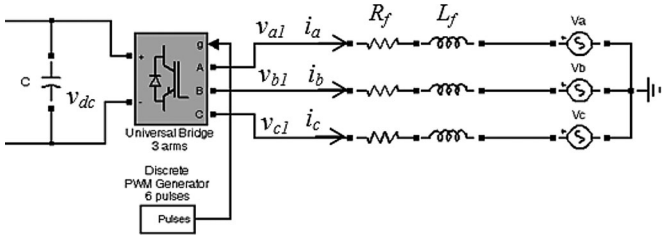

Fig. 4. GSC schematic.

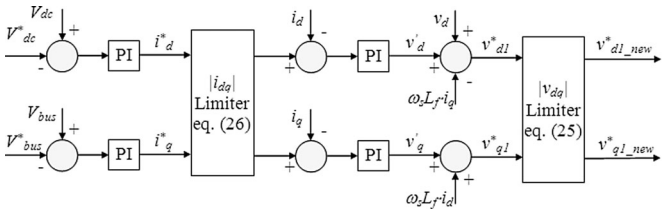

Fig. 5. Conventional standard GSC vector control structure.

and i_q represent the d- and q-axis components of the current flowing between the GSC and the ac system.

In the PCC voltage oriented frame [12], [13], [18], [19], the instantaneous active and reactive powers transferred from the GSC to the grid are proportional to grid d- and q-axis currents, respectively, as shown by (19) and (20), while the steady-state active and reactive powers are proportional to the GSC q- and d-axis output voltages V_{d1} and V_{q1}, respectively, as shown by (21) [17]

$$p(t) = v_d i_d + v_q i_q = v_d i_d \tag{19}$$

$$q(t) = v_q i_d - v_d i_q = -v_d i_q \tag{20}$$

$$P = V_d V_{q1}/X_f, \quad Q = V_d\left(V_{d1} - V_d\right)/X_f. \tag{21}$$

B. Conventional Vector Control of GSC

The conventional vector control method for the GSC has a nested-loop structure consisting of a faster inner current loop and a slower outer loop as shown by Fig. 5 [12], [17], [35], in which the d-axis loop is used for dc-link voltage control, and the q-axis loop is used for reactive power or grid voltage support control. The control strategy of the inner current loop is developed by rewriting (18) as

$$v_{d1} = \left(R_f i_d + L_f \cdot di_d/dt\right) - \omega_s L_f i_q + v_d \tag{22}$$

$$v_{q1} = \left(R_f i_q + L_f \cdot di_q/dt\right) + \omega_s L_f i_d \tag{23}$$

in which the item in the bracket of (22) and (23) is treated as the state equation between the voltage and current on d- and q-axis loops, and the other items are treated as compensation terms [12], [35]. This treatment assumes that v_{d1} in (22) has no major influence on i_q, and v_{q1} in (23) has no significant impact on i_d.

However, this assumption conflicts with the GSC power control relations. According to Fig. 5, the final control voltages v^*_{d1} and v^*_{q1}, linearly proportional to the converter output voltages V_{d1} and V_{q1} [25], include the d- and q-axis voltages v'_d and v'_q generated by the current-loop controllers plus the compensation terms as shown by (24). Hence, the conventional GSC control configuration intends to regulate i_d and i_q using v'_d and v'_q, respectively. But, according to (19)–(21), the d-axis voltage is only effective for reactive power or i_q control, and the q-axis voltage is only effective for active power or i_d control.

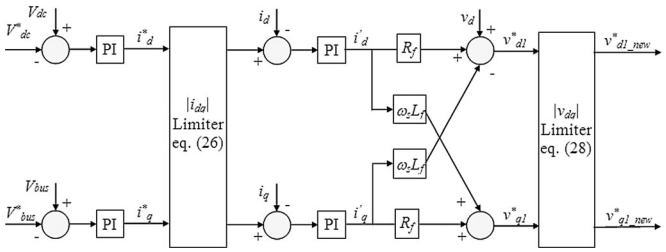

Fig. 6. Direct-current vector control structure for a PMSG GSC.

$$v^*_{d1} = v'_d - \omega_s L_f i_q + v_d, \quad v^*_{q1} = v'_q + \omega_s L_f i_d. \tag{24}$$

The following issues are considered in the design of the conventional GSC controller.

1) To prevent the GSC from exceeding the PWM saturation limit, (25) is applied if the amplitude of the reference voltage generated by the inner current-loop controller exceeds the converter PWM saturation limit [17], [36], where $v^*_{\mathrm{d1\_new}}$ and $v^*_{q1\_\mathrm{new}}$ are the d- and q-component of the modified controller output voltage, and $V_{\mathrm{max\_GSC}}$ is the maximum allowable dq voltage. It is found that any other modification mechanisms can result in increased system oscillation and unbalance

$$\begin{aligned} v^*_{d1\_\mathrm{new}} &= V_{\mathrm{max\_GSC}} \cos\left(\angle v^*_{dq1}\right) \\ v^*_{q1\_\mathrm{new}} &= V_{\mathrm{max\_GSC}} \sin\left(\angle v^*_{dq1}\right). \end{aligned} \tag{25}$$

2) To prevent the GSC from exceeding the rated current, (26) is employed if the amplitude of the reference current generated by the outer control loop exceeds the rated current limit, i.e., keeping the d-axis current reference i^*_d unchanged to maintain dc-link voltage control effectiveness while modifying the q-axis current reference i^*_q to satisfy the reactive power or ac system bus voltage support control demand as much as possible [17], [36]

$$\begin{aligned} i^*_{d\_\mathrm{new}} &= i^*_d \\ i^*_{q\_\mathrm{new}} &= \mathrm{sign}\left(i^*_q\right) \cdot \sqrt{\left(i^*_{dq\_\max}\right)^2 - \left(i^*_d\right)^2}. \end{aligned} \tag{26}$$

C. Direct-Current Vector Control of GSC

The direct-current vector control strategy of the GSC (see Fig. 6) is implemented through a nested-loop controller in the following way: 1) transforming the dc-link voltage and reactive power control to d- and q-axis current control; 2) developing a direct current control scheme; and 3) converting current control signals to voltage control signals [19].

First, according to (19) and (20), the dc-link voltage control is transformed to d-axis current control through a dc-link voltage controller, and the ac system reactive power control is transformed to q-axis current control through a reactive power

controller. Second, an inner current-loop controller is developed based on a direct-current vector control mechanism by generating d- and q-axis tuning current signals i'_d and i'_q through an adaptive tuning strategy [31]–[33]. The purpose of the current-loop controller is to assure the highest power quality of the ac system in terms of harmonics and unbalance. Therefore, similar to Section III-D, elimination of the current loop [37], [38] is not an option for GSC control. Third, the d and q-tuning current signals i'_d and i'_q generated by the current-loop controllers are transferred to d- and q-voltage signals v^*_{d1} and v^*_{q1} due to the VSC structure for the GSC. The conversion from the current to voltage control signals is implemented through

$$v^*_{d1} = R_f i'_d - \omega_s L_f i'_q + v_d, \quad v^*_{q1} = R_f i'_q + \omega_s L_f i'_d. \quad (27)$$

Signal processing technology is applied to the measured voltages and currents in Fig. 6. In addition, a nonlinear programming strategy is employed to prevent the GSC from exceeding the rated current and to prevent the converter from entering the nonlinear modulation mode as shown in the following, where $I_{\mathrm{GSC\_rated}}$ is the rated GSC phase rms current and Q^*_{ac} is the reference reactive power of the GSC. The basic principle of the nonlinear programming strategy is to minimize the error between the actual and desired reactive powers, subject to constraints that force the dc-link voltage to the reference value, limit the GSC rms phase current to the rated current, and maintain GSC PWM saturation limits.

Minimize: $|Q_{\mathrm{ac}} - Q^*_{\mathrm{ac}}|$

Subject to: $V_{\mathrm{dc}} = V^*_{\mathrm{dc}}, \sqrt{\left(I_d^2 + I_q^2\right)/3} \le I_{\mathrm{GSC\_rated}}$

$$\sqrt{\left(V_{d1}^2 + V_{q1}^2\right)/3} \le V_{\mathrm{dc}} \Big/ \left(2\sqrt{2}\right).$$

The nonlinear programming strategy is implemented in the following way. If $\left|i^*_{dq}\right|$ generated by the outer dc-link voltage and reactive power control loops exceeds the rated current limit, i^*_d and i^*_q are modified by (26). If $\left|v^*_{dq1}\right|$ generated by the inner current control loops exceeds the converter PWM saturation limit, the d- and q-axis voltages are recalculated by (28). In fact, according to (21), (28) represents an optimal control strategy for keeping the q-axis voltage reference v^*_{q1} unchanged so as to maintain the dc-link voltage control effectiveness while modifying the d-axis voltage reference v^*_{d1} to meet the reactive power or ac system bus voltage support control demand as much as possible.

$$v^*_{d1\_\mathrm{new}} = \mathrm{sign}\left(v^*_{d1}\right) \cdot \sqrt{\left(v^*_{dq1\_\max}\right)^2 - \left(v^*_{q1}\right)^2}$$
$$v^*_{q1\_\mathrm{new}} = v^*_{q1}. \quad (28)$$

V. MSC and GSC for Integrated Wind Turbine Control

The key requirements for integrated PMSG wind turbine control include 1) maximum wind power extraction control; 2) dc-link voltage control; 3) reactive power control; and 4) grid voltage support control.

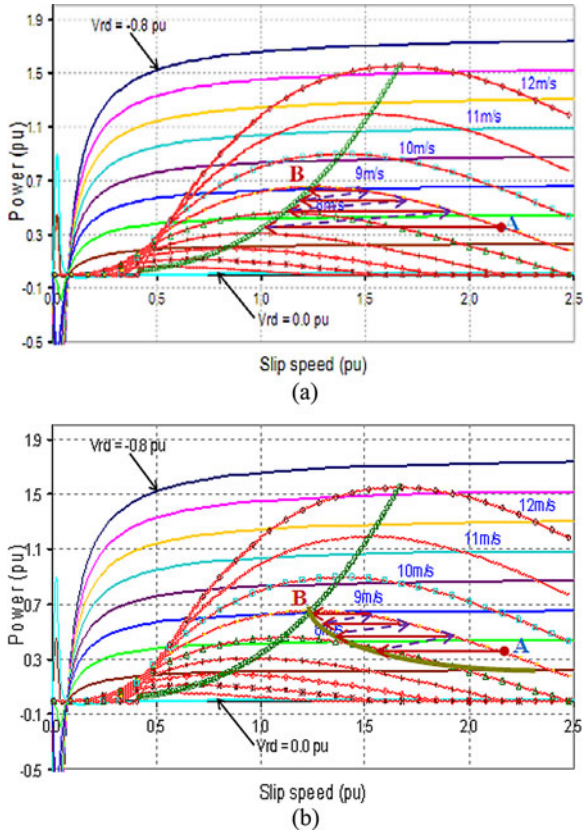

Fig. 7. Lookup table approach for PMSG maximum power extraction ($V_{sq} = 0.7$ p.u., $p = 150$, $\beta = 1°$). (a) Direct lookup table approach. (b) Virtual lookup table approach.

A. Maximum Wind Power Extraction Control

For a given wind speed, the goal of the maximum power extraction is to regulate the turbine rotating speed to ω_{m_opt} so that the maximum power can be captured from the wind. The existing commercial peak power tracking control strategy for a DFIG wind turbine [19], [39]–[41], requiring no wind speed information, uses wind turbine output power and a P–ω lookup table to generate speed references for the DFIG speed-loop controller in a recursive manner. However, this lookup table approach, when applied to a PMSG wind turbine, may cause unstable operation of the wind turbine. This can be explained in Fig. 7(a) through integrated generator converted power, extracted wind power, and maximum power extraction characteristics [16]. For each wind speed, from the generator converted power and extracted wind power characteristic standpoint, only the intersection of the two characteristics at the higher speed point on the right side in Fig. 7(a) is dynamically stable. Nevertheless, the speed references generated from the maximum power extraction P–ω curve have a tendency to bring a PMSG into an unstable operating mode on the left side in Fig. 7(a). It is found that, in a transient feedback control environment [16], the conventional P–ω lookup table approach suitable to a DFIG wind turbine could result in significant oscillations and instability of a PMSG wind turbine.

This paper employs an adaptive virtual lookup table approach for PMSG maximum power extraction control [see Fig. 7(b)], which requires not only turbine output power but also generator rotating speed. For example, assuming that a PMSG operates initially at point A in Fig. 7(b), when the wind speed is 9 m/s, then based on the measured PMSG output power $P_{\text{grid}}^{\text{mea}}$, a recursive process starts. 1) The peak power tracking approach generates a speed reference to the speed-loop controller based on a virtual *P*–ω curve. 2) The controller responds to the reference change by decreasing the generator speed, which causes more power output. 3) The peak power tracking approach generates a new speed reference due to the output power increase. The process continues until the peak power point B is reached. The special features of the virtual loopup table approach include the following.

1) A virtual lookup table. The speed reference generated from the peak power tracking strategy involves two steps. First, for each measured turbine output power, generate a speed reference from the conventional *P*–ω curve [see Fig. 7(b)]. Second, adjust the speed reference by considering the difference between the generator rotating speed and the speed reference obtained from the *P*–ω curve so that the updated speed reference to the speed-loop controller will assure stable operation of the generator.
2) Dynamic formation of the virtual lookup table. Unlike the traditional fixed *P*–ω curve, the virtual *P*–ω lookup table has different dynamic traces for transition from different PMSG operating points toward a maximum power extraction speed point [see Fig. 7(b)].

In general, the speed reference of the proposed approach is calculated using (29), where $\omega_{\text{table}}^{*}$ is the reference speed generated by the conventional *P*–ω lookup table, and k is a coefficient between 0 and 1. Actually, when $k = 0$, $\omega^{*} = \omega_{\text{table}}^{*}$; when $k = 1$, $\omega^{*} = \omega_{m}$; when $0 < k < 1$, $\omega_{\text{table}}^{*} < \omega^{*} < \omega_{m}$. During the operation of the machine, the value of k is determined through a nonlinear function of $(\omega_{m} - \omega_{\text{table}}^{*})$ (29). As the PMSG operating speed is close to $\omega_{\text{table}}^{*}$, the value of k should be smaller. It is also possible to determine k through a fuzzy or an adaptive rule. Therefore, a dynamic and virtual lookup table will be formed during the maximum power extraction control of a PMSG wind turbine

$$\omega^{*} = \omega_{\text{table}}^{*} + k \cdot (\omega_{m} - \omega_{\text{table}}^{*}), \quad k = f\ (\omega_{m} - \omega_{\text{table}}^{*}). \tag{29}$$

B. DC-Link Voltage Control

For a PMSG wind turbine, the full power captured from the wind has to be transferred through the dc link and the GSC to the grid. This situation is different from that of a DFIG wind turbine. Because of this, control of the dc-link voltage is more challenging for a PMSG wind turbine than a DFIG wind turbine, especially when the conventional vector control structure (see Fig. 5) is used for the dc-link voltage control. However, when using the direct-current vector control structure for the GSC (see Fig. 6), high performance and fast dc-link voltage control can be obtained. Thus, control functions of the MSC and GSC can be decoupled effectively with the MSC responsible for maximum power extraction control and the GSC responsible for the dc-link voltage control so that energy captured from the wind can be transferred to the grid while the dc-link voltage is stable (see Section VI).

C. Reactive Power or PCC Voltage Support Control

In addition to dc-link voltage control, the GSC also contributes to grid reactive power or PCC voltage support control [42]. In the reactive power control mode, the q-axis reference current is generated through a reactive power controller. In the ac system voltage support control mode, the q-axis reference current is generated through a PCC voltage controller, during which the GSC should generate a reactive power as much as possible depending on how much the PCC voltage drops. In the integrated MSC and GSC control environment, if the GSC reaches its physical constraints due to a high active power transferred from the synchronous generator through the GSC to the grid, the GSC operates in the optimal control mode, i.e., maintaining the dc-link voltage as the first priority while meeting GSC reactive power or grid voltage support control demand as much as possible. But, this optimal control mechanism cannot be applied to the conventional GSC control structure (see Fig. 5), which can result in large oscillations and unbalances of the overall system due to its competing control nature [17].

VI. Performance Evaluation and Comparison

To evaluate the peak power tracking, reactive power, and grid voltage support controls of a PMSG wind turbine using both conventional and proposed control strategies, an integrated transient simulation of a complete PMSG system including the MSC and GSC is developed by using power converter average and detailed models in SimPowerSystems (see Fig. 8), in which both steady and variable wind conditions are considered. The average model is used for an initial evaluation while the detailed switching model (see Fig. 8) is used for more practical investigation. For the switching-model-based PMSG system, losses within power converters are considered. The parameters used in the simulation study are shown in Tables I and II. The grid impedance is the equivalent impedance referred to a PMSG wind turbine by considering the effect of 100 wind turbines operating at the same condition [40], [43]. The converter switching frequency is 1980 Hz for both the GSC and MSC. All the results presented in this paper are generated from the switching-model-based simulation.

A. Peak Power Tracking and Reactive Power Control

Fig. 9 demonstrates a case study of peak power tracking and reactive power control under a steady wind condition using the direct-current vector control strategy for both the GSC and MSC. Before $t = 6$ s, the wind speed is 7 m/s, and the reactive power reference at the PCC is 0 kvar. After the system is settled, the output power of the wind turbine is very close to the maximum power that can be captured by the turbine at this wind speed [see Fig. 9(b)]. The net reactive power is effectively maintained at the reactive power reference [see Fig. 9(b)], and the

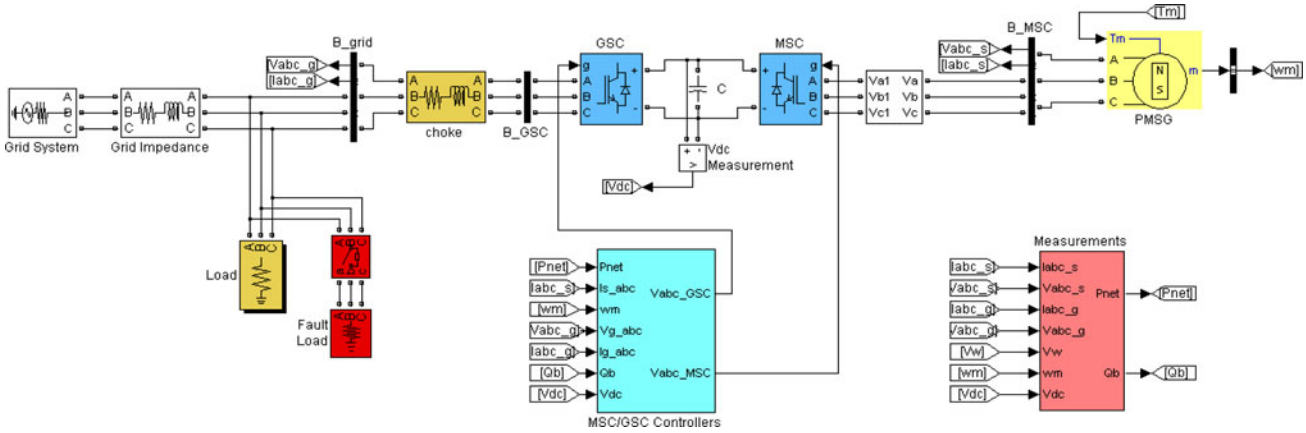

Fig. 8. MSC and GSC control of a PMSG wind turbine in SimPowerSystems.

dc-link voltage is stabilized at the desired dc voltage reference of 1500 V [see Fig. 9(d)]. It is necessary to indicate that a low generator rotating speed [see Fig. 9(a)] is due to a large generator pole number for a direct-driven PMSG wind turbine. At $t = 6$ s when the grid reactive power demand changes to 200 kvar (generating), the net reactive power of the wind turbine quickly reaches the new reactive power reference [see Fig. 9(b)]. The dc-link voltage is almost unaffected [see Fig. 9(d)], showing the excellent performance of the system under the direct-current vector control configuration. At $t = 8$ s, as the wind speed increases from 7 to 9 m/s, the peak power tracking strategy recursively generates the reference generator speed [see Fig. 9(a)] while the MSC controller regulates the generator speed and turbine output power smoothly until the new maximum power point is reached [see Fig. 9(a) and (b)]. With more power captured from the wind under a higher wind speed, the stator q-axis current i_{sq} increases, but the stator d-axis current i_{sd} remains zero (minimum stator current control). This yields increased power transfer to the dc-link capacitor, causing the dc-link voltage to increase [see Fig. 9(d)]. But, the direct-current vector control of the GSC quickly stabilizes the dc-link voltage to the reference value [see Fig. 9(d)]. At $t = 11$ s, when the reactive power reference changes to 500 kvar, the controller output voltage of the GSC is over the PWM saturation limit. Therefore, the GSC transitions to the optimal control mode by maintaining a constant dc-link voltage as the first priority while generating reactive power as much as possible [see Fig. 9(f)]. At $t = 14$ s, as the wind speed changes from 9 to 8 m/s, the power transferred from the MSC to the GSC drops so that the GSC is able to generate more reactive power under the optimal control strategy [see Fig. 9(b)]. At $t = 17$ s, as the reactive power reference reduces to 300 kvar, the GSC returns to its normal control mode. For any other reactive power reference and wind speed variations, the integrated GSC and MSC control performs effectively for maximum power extraction, reactive power, and dc-link voltage controls with high power quality on the three-phase stator currents of the generator and the three-phase currents at the PCC [see Fig. 9(g) and (h)].

For the same condition using the conventional vector control method, the PMSG system performance (see Fig. 10) is close to Fig. 9 before $t = 8$ s. As the wind speed changes from 7 to 9 m/s at $t = 8$ s, a much higher variation of the dc-link voltage [see Fig. 10(d)] is found due to the increase of the power transferred from the PMSG to the dc-link capacitor. At $t = 11$ s, when the reactive power reference changes to 500 kvar, the controller output voltage of the GSC is over the PWM saturation limit. Therefore, the GSC operates according to (25), which may make the power transferred from the PMSG to the dc-link capacitor unable to pass to the grid. This situation could result in a variable dc-link voltage and malfunction of the PMSG wind turbine as shown in Fig. 10 after $t = 11$ s. It is also found that when the PWM saturation limit is exceeded during MSC control, instability or malfunction of the PMSG wind energy extraction control could be present when using the conventional MSC vector control technique [15].

B. Peak Power Tracking and Voltage Support Control

Figs. 11 and 12 present PCC voltage support control using the proposed control method for low and high voltage drop conditions, respectively. In both figures, the wind speed is 7 m/s and a voltage drop is generated in the simulation between 10 and 12 s while the rest conditions are the same as those used in Fig. 9. The performance of the voltage support control of a PMSG wind turbine depends on how great the voltage drop is and how much power is transferred from the PMSG to the grid.

For a low voltage drop on the PCC bus (see Fig. 11) at a low wind speed, the integrated GSC and MSC control works properly for peak power tracking [see Fig. 11(b)], dc-link voltage control [see Fig. 11(e)], and PCC bus voltage support control [see Fig. 11(f)]. At the start of the voltage drop, there is a sudden change of the PCC bus voltage [see Fig. 11(f)], causing a spike in the instantaneous active and reactive power transferred to the grid due to a distortion of the grid three-phase current. However, the integrated GSC and MSC control, under the direct-current vector control structure, quickly stabilizes the dc-link voltage and restores the PCC bus voltage to the rated value. During the voltage support control period, the PMSG maximum power extraction is not affected much [see Fig. 11(b) and (c)]. Thus, the GSC d-axis current i_d remains almost unchanged while the

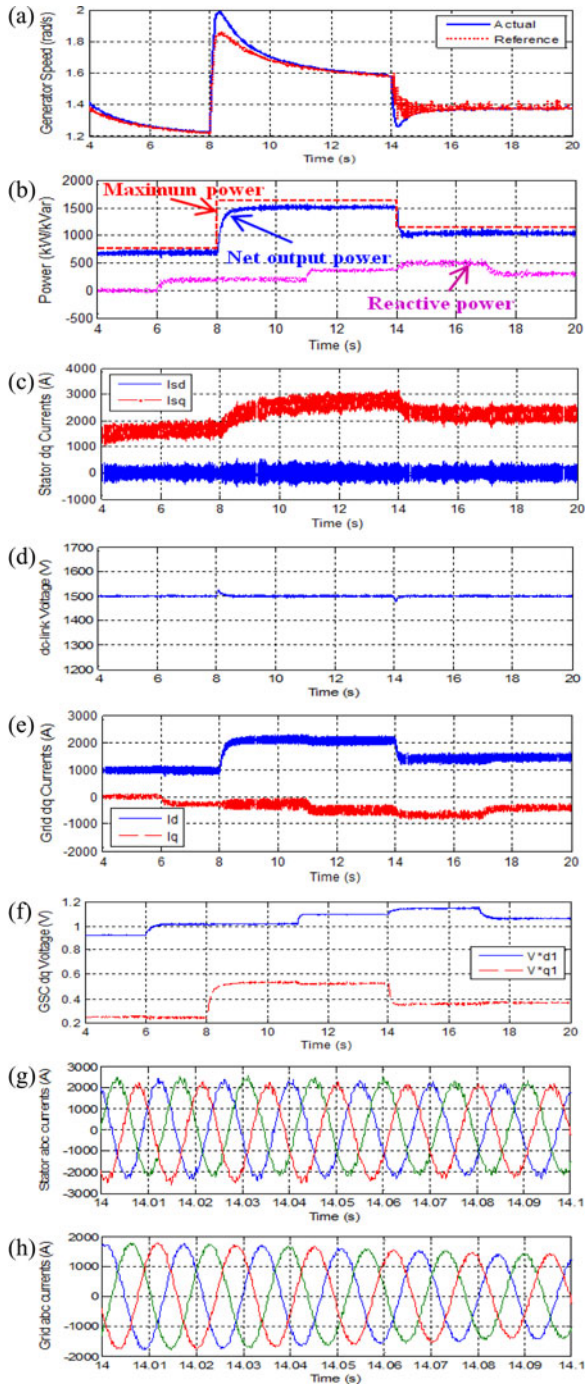

Fig. 9. GSC and MSC for peak power tracking and reactive power controls of a PMSG wind turbine (proposed).

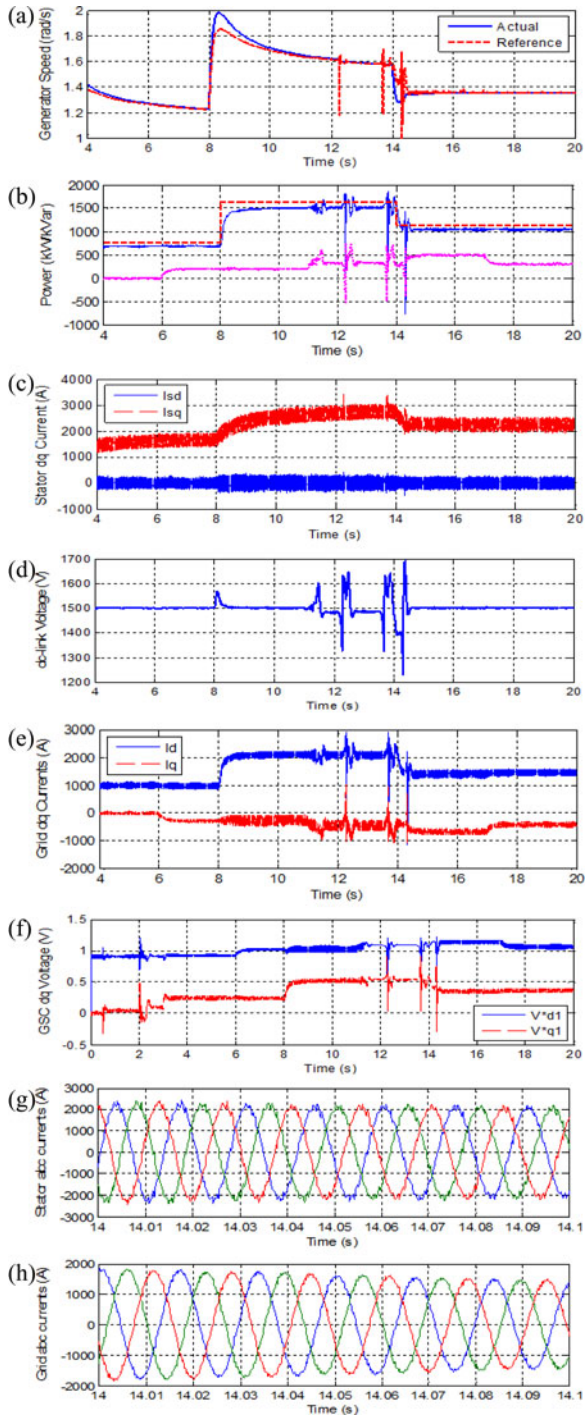

Fig. 10. GSC and MSC for peak power tracking and reactive power controls of a PMSG wind turbine (conventional).

q-axis current i_q becomes more negative to generate reactive power to meet the PCC bus voltage support control need. When the voltage drop is cleared at $t = 12$ s, there is a boost of the PCC bus voltage. But the integrated GSC and MSC control under the direct-current vector control configuration quickly reduces the reactive power generation and restores the PMSG system to normal operation with very small oscillations.

For a moderate voltage drop on the PCC bus (see Fig. 12), more reactive power generation is needed to boost the PCC voltage. However, due to the rated current or converter PWM saturation constraint, the GSC, unable to generate the required reactive power, operates in the optimal control mode by maintaining the dc-link voltage as the first priority [see Fig. 12(e)] while generating the reactive power as much as possible [see Fig. 12(b) and (d)]. Therefore, the final PCC bus voltage is lower than the rated PCC voltage of 1 p.u. [see Fig. 12(f)]. Since the dc-link voltage is kept almost constant under the

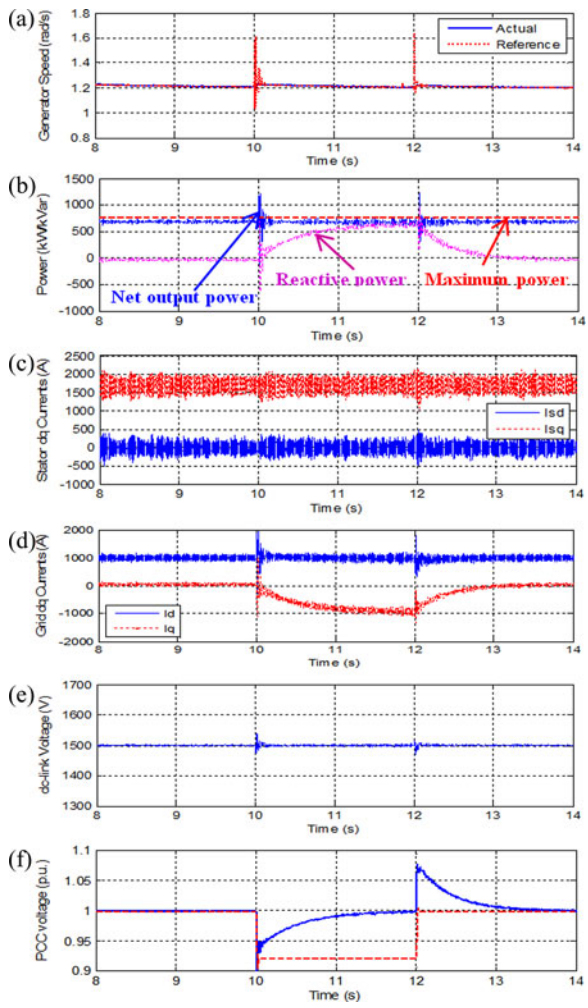

Fig. 11. GSC and MSC for maximum power extraction and voltage support controls during a low voltage drop.

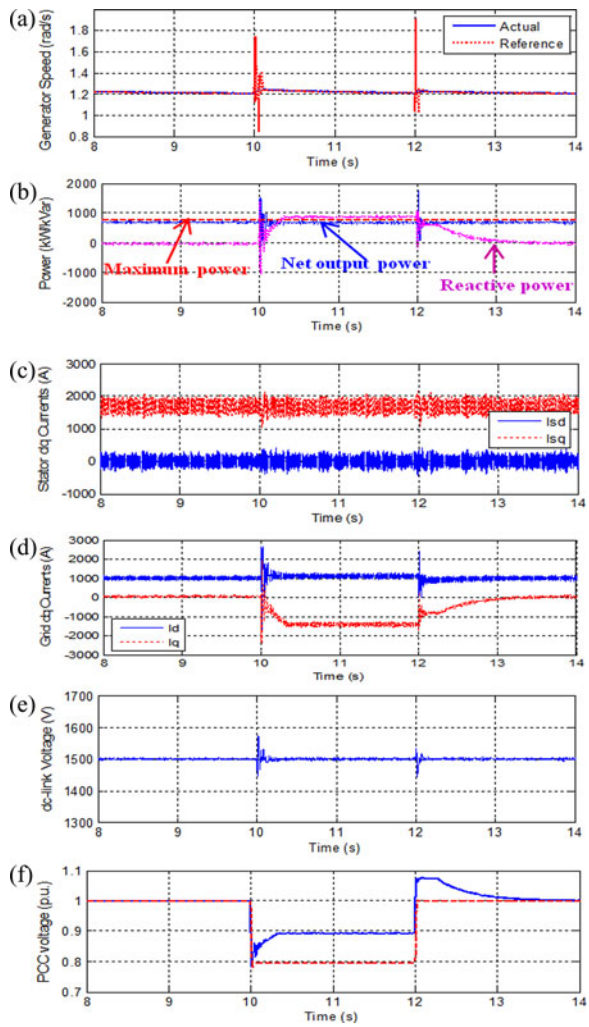

Fig. 12. GSC and MSC for maximum power extraction and voltage support controls during a moderate voltage drop.

optimal and direct-current vector control strategy, the operation of the synchronous generator and the maximum wind power extraction is nearly unaffected [see Fig. 12(a)–(c)], demonstrating strong short-circuit ride through capability of the PMSG wind turbine under the direct-current vector control configuration.

C. GSC and MSC Control Under Variable and Gusty Wind

In reality, wind speed changes constantly over the time. Over periods shorter than 1 h, wind speed can be approximated as the superposition of a slowly varying mean speed V_w plus N sinusoidal components having frequencies ω_i, amplitudes A_i, and random phases ϕ_i as shown by [44]

$$v_w(t) = V_w + \sum_{i=1}^{N} A_i \cos(\omega_i t + \phi_i). \tag{30}$$

In (30), ω_i is a random variable that has Von Karman distribution described by (31), where L represents the roughness of the area around the wind turbine, and σ is the standard deviation of the wind speed distribution. The amplitude A_i of each discrete frequency component, chosen to give it a power equal to that contained in a certain frequency band, is calculated by (32), [44]

$$S_{vv}(\omega_i) = \frac{0.475\sigma^2\,(L/V_w)}{\left[1 + (\omega_i L/V_w)^2\right]^{5/6}} \tag{31}$$

$$A_i(\omega_i) = \sqrt{\left(S_{vv}(\omega_i) + S_{vv}(\omega_{i+1})\right)(\omega_{i+1} - \omega_i)}. \tag{32}$$

Figs. 13 and 14 show the performance of integrated GSC and MSC control for peak power tracking, dc-link voltage regulation, and reactive power control under variable and gusty wind conditions using the proposed and conventional control methods. The reactive power reference is 0 kvar while all other conditions are similar to those used in Fig. 9. Before $t = 10$ s, the wind speed is 7 m/s. At $t = 10$ s, the wind speed is generated using (30)–(32) with $V_w = 7$ m/s, which results in variable and short-term gusty winds. Due to the low wind speed and reactive power demand, the GSC and MSC of the PMSG turbine always operate within the PWM saturation limits. Under varying wind conditions, the maximum available power that

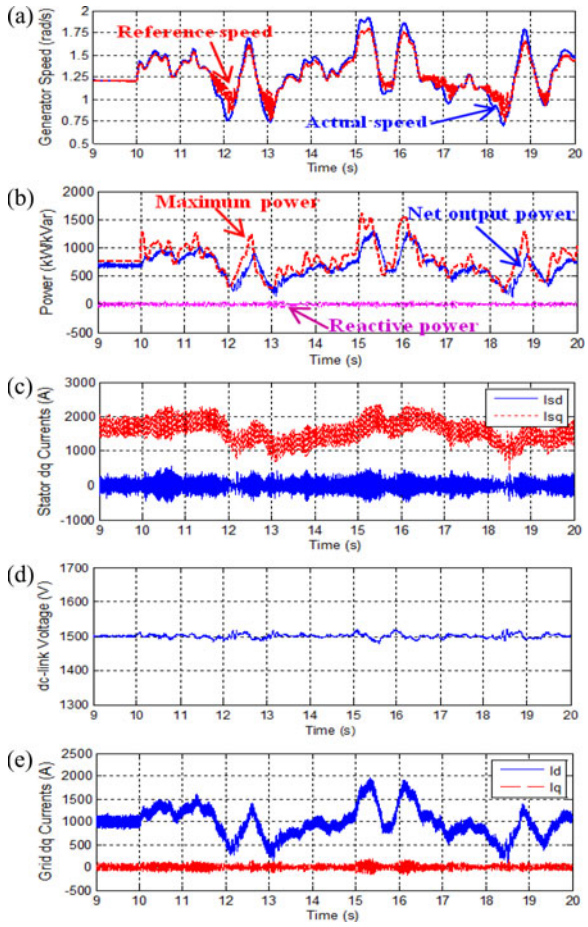

Fig. 13. GSC and MSC for peak power tracking and reactive power controls under variable and gusty wind (proposed).

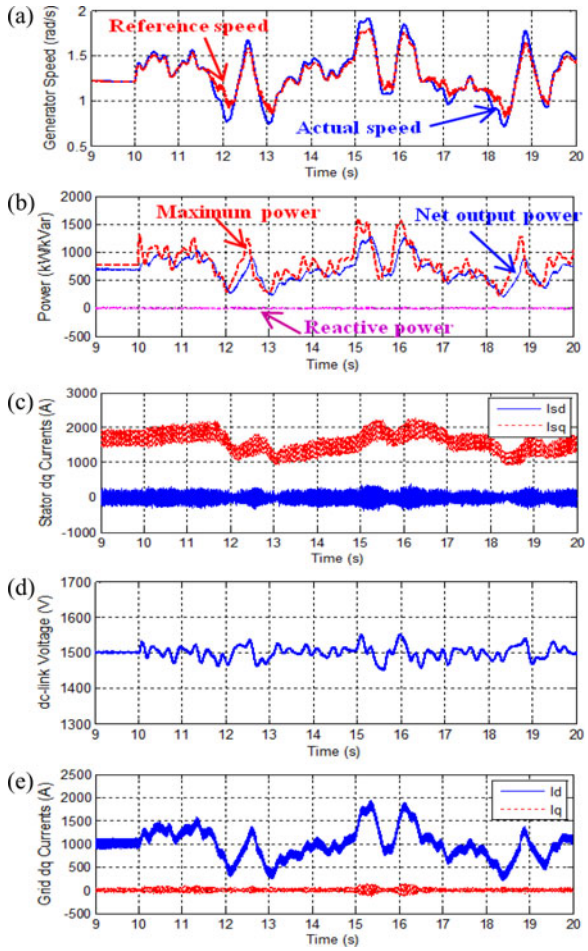

Fig. 14. GSC and MSC for peak power tracking and reactive power controls under variable and gusty wind (conventional).

can be extracted by a PMSG wind turbine fluctuates sharply. However, the turbine rotating speed and net output power shift smoothly using the recursive virtual lookup table peak power tracking control strategy (see Figs. 13 and 14). The net output power of the wind turbine properly follows the maximum available power while the influence of the gusting wind is restrained as shown by Figs. 13(b) and 14(b), demonstrating the effectiveness and stability of the recursive peak power tracking mechanism in variable and gusty wind conditions. The stator q-axis current i_{sq} changes with the wind speed for maximum power extraction while the stator d-axis current i_{sd} is maintained at zero [see Figs. 13(c) and 14(c)]. The variation of the active power transferred from the synchronous generator to the grid through the GSC causes an oscillating dc-link voltage. But in the optimal and direct-current vector control configuration, the dc-link voltage is properly maintained around the reference voltage with minimal fluctuation [see Fig. 13(d)]. Nevertheless, by using the conventional control method, the oscillation of the dc-link voltage is more evident [see Fig. 14(d)], which may require control of generator speed to achieve a stable dc-link voltage [45].

VII. Conclusion

This paper presents and compares conventional and a novel direct-current vector control designs for a PMSG wind turbine. This paper shows how integrated GSC and MSC control is designed by using the conventional and direct-current vector control configurations to implement the maximum power extraction, dc-link voltage regulation, reactive power control, and grid voltage support control of a PMSG wind turbine.

Comprehensive simulation studies demonstrate that a PMSG wind turbine, based on the direct-current vector control structure, can effectively accomplish the wind turbine control objectives with superior performance within the physical constraints of the system under both steady and variable wind conditions. Beyond the physical constraints of a PMSG system, the proposed control approach operates in an optimal mode by controlling the MSC for maximum wind power extraction as the first priority and controlling the GSC to stabilize the dc-link voltage as the main concern. However, if the output voltage of the current-loop controller at either the MSC or GSC exceeds the PWM saturation limit, the conventional control mechanism could result in unstable operation or malfunction of the PMSG system.

The direct-current vector current structure is also effective for peak power tracking and grid voltage support control under low voltage drop conditions caused by a fault or load change. But, for a high PCC bus voltage drop, it may be impossible to boost the PCC voltage to the rated bus voltage because of the rated current and converter PWM saturation constraints. Compared to a DFIG wind turbine, the voltage drop influence on a PSMG wind turbine is much smaller, demonstrating superior fault-ride through capability of a PMSG system under the direct-current vector control configuration.

APPENDICES

TABLE I
PARAMETER OF THE PMSG WIND TURBINE

Parameter	Value	Units
S_g (Generator rated power)	2500	kVA
f (frequency)	60	Hz
V_g (Generator rated Voltage)	575	V
R_s (stator resistance)	0.0025	p.u.
L_{ls} (stator leakage inductance)	0.02	p.u.
Mutual inductance in d-axis, L_{dm}	0.43	p.u.
Mutual inductance in q-axis, L_{qm}	0.48	p.u.
Permanent magnet flux	1.0	p.u.
C (dc-link capacitor)	60000	μF
R_f (grid-filter resistance)	0.0012	Ω
L_f (grid-filter inductance)	0.5	mH

TABLE II
RELEVANT DATA OF A WIND POWER PLANT

Equipment	Voltage ratio	R (pu)	X (pu)	Base Power
Wind turbine transformer	0.69/36KV	0.8%	4.52%	2MW
PCC transformer	36/200KV	0.5%	6.5%	150MW
Transmission line	200KV	2.54%	11.9%	300MW
Grid transformer	200/400kV	0.024%	2.4%	150MW

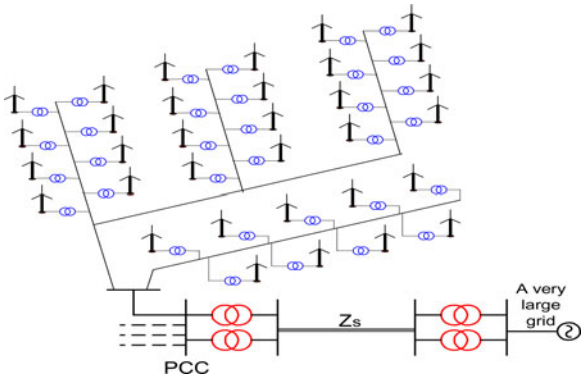

Fig. A1. Illustration of a wind power plant.

REFERENCES

[1] R. Zavadil, N. Miller, A. Ellis, and E. Muljadi, "Making connections: Wind generation challenges and progress," *IEEE Power Energy Mag.*, vol. 3, no. 6, pp. 26–37, Nov. 2005.
[2] Z. Chen, J. M. Guerrero, and F. Blaabjerg, "A review of the state of the art of power electronics for wind turbines," *IEEE Trans. Power Electron.*, vol. 24, no. 8, pp. 1859–1875, Aug. 2009.
[3] S. Jöckel, "High energy production plus built in reliability—The new Vensys 70/77 gearless wind turbines in the 1.5 MW class," presented at the 2006 Eur. Wind Energy Conf., Athens, Greece, Feb. 27–Mar. 2, 2006.
[4] Y. Chen, P. Pillary, and A. Khan, "PM wind generator topologies," *IEEE Trans. Ind. Appl.*, vol. 41, no. 6, pp. 1619–1626, Nov./Dec. 2005.
[5] H. Polinder, S. W. H. de Haan, M. R. Dubois, and J. Slootweg, "Basic operation principles and electrical conversion systems of wind turbines," presented at the Nordic Workshop Power Ind. Electron., Trondheim, Norway, Jun. 14–16, 2004.
[6] G. Michalke, A. D. Hansen, and T. Hartkopf, "Control strategy of a variable speed wind turbine with multipole permanent magnet synchronous generator," presented at the 2007 Eur. Wind Energy Conf. Exhib., Milan, Italy, May 7–10, 2007.
[7] A. Grauers, "Efficiency of three wind energy generator systems," *IEEE Trans. Energy Convers.*, vol. 11, no. 3, pp. 650–657, Sep. 1996.
[8] K. Tan and S. Islam, "Optimum control strategies in energy conversion of PMSG wind turbine system without mechanical sensors," *IEEE Trans. Energy Convers.*, vol. 19, no. 2, pp. 392–399, Jun. 2004.
[9] F. Velenciaga and P. F. Puleston, "High-order sliding control for a wind energy conversion system based on a permanent magnet synchronous generator," *IEEE Trans. Energy Convers.*, vol. 23, no. 3, pp. 860–867, Sep. 2008.
[10] North American Electric Reliability Corporation. (2009 Apr.) Accommodating High Levels of Variable Generation [Online]. Available: http://www.nerc.com/files/IVGTF_Report_041609.pdf
[11] Clipper Windpower, The Liberty 2.5 MW Wind Turbine: Clipper Design. (Dec. 2011). [Online]. Available: http://www.clipperwind.com/productline.html
[12] J. Belhadj and X. Roboam, "Investigation of different methods to control a small variable-speed wind turbine with PMSM drives," *J. Energy Resources Technol.*, vol. 129, pp. 200–213, Sep. 2007.
[13] M. Chinchilla, S. Arnaltes, and J. C. Burgos, "Control of permanent-magnet generators applied to variable-speed wind-energy systems connected to the grid," *IEEE Trans. Energy Convers.*, vol. 21, no. 1, pp. 130–135, Mar. 2006.
[14] W. Qiao, L. Qu, and R. G. Harley, "Control of IPM synchronous generator for maximum wind power generation considering magnetic saturation," *IEEE Trans. Ind. Appl.*, vol. 45, no. 3, pp. 1095–1105, Jun. 2009.
[15] S. Li, T. A. Haskew, and L. Xu, "Conventional and novel control designs for direct driven PMSG wind turbines," *Electr. Power Syst. Res.*, vol. 80, no. 3, pp. 328–338, Mar. 2010.
[16] S. Li, T. A. Haskew, and Y. Hong, "PMSG maximum wind power extraction control using adaptive virtual lookup table approach in direct-current vector control structure," *Int. J. Energy Res.*, vol. 35, no. 11, pp. 929–1022, Sep. 2011.
[17] S. Li, T. A. Haskew, and L. Xu, "Control of HVDC light systems using conventional and direct-current vector control approaches," *IEEE Trans. Power Electron.*, vol. 25, no. 12, pp. 3106–3118, Dec. 2010.
[18] J. Matas, M. Castilla, J. M. Guerrero, L. Garcia de Vicuna, and J. Miret, "Feedback linearization of direct-drive synchronous wind-turbines via a sliding mode approach," *IEEE Trans. Power Electron.*, vol. 23, no. 3, pp. 1093–1103, May 2008.
[19] A. D. Hansen, P. Sørensen, F. Iov, and F. Blaabjerg, "Control of variable speed wind turbines with doubly-fed induction generators," *Wind Eng.*, vol. 28, no. 4, pp. 411–432, Jun. 2004.
[20] A. R. Bergen and V. Vittal, *Power System Analysis*, 2nd ed. Upper Saddle River, NJ: Prentice-Hall, 2000.
[21] M. B. Bana Sharifian, Y. Mohamadrezapour, M. Hosseinpour, and S. Torabzade, "Maximum power control of variable speed wind turbine connected to permanent magnet synchronous generator using chopper equipped with superconductive inductor," *J. Appl. Sci.*, vol. 9, no. 4, pp. 777–782, 2009.
[22] D. J. Bang, H. Polinder, G. Shrestha, and J. A. Ferreira, "Review of generator systems for direct-drive wind turbines," presented at the Eur. Wind Energy Conf. Exhib., Belgium, Mar. 31–Apr. 3, 2008.

[23] S. Heier, *Grid Integration of Wind Energy Conversion Systems*, 2nd ed. New York: Wiley, 2006.
[24] N. W. Miller, W. W. Price, J. J. Sanchez-Gasca. (2003, Oct. 27). Dynamic modeling of GE 1.5 and 3.6 wind turbine-generators Version 3.0, Tech. Rep., GE Power Systems Energy Consulting, Schenectady, NY, [Online]. Available: http://www.easthavenwindfarm.com/filing/high/modeling.pdf 2012.
[25] N. Mohan, *Advanced Electric Drives—Analysis, Modeling and Control Using Simulink,* Minnesota Power Electronics Research & Education, MN, 2001.
[26] R. Gagnon. "Detailed Model of a Doubly-Fed Induction Generator (DFIG) Driven by a Wind Turbine," The MathWorks, Inc., Natick, MA, Jan. 2006.
[27] D. Santos-Martin, J. L. Rodriguez-Amenedo, and S. Arnalte, "Direct power control applied to doubly fed induction generator under unbalanced grid voltage conditions," *IEEE Trans. Power Electron*., vol. 23, no. 5, pp. 2328–2336, Sep. 2008.
[28] J. A. Restrepo, J. M. Aller, J. C. Viola, A. Bueno, and T. G. Habetler, "Optimum space vector computation technique for direct power control," *IEEE Trans. Power Electron*., vol. 24, no. 6, pp. 1637–1645, Jun. 2009.
[29] P. Zhou, Y. He, and D. Sun, "Improved direct power control of a DFIG-based wind turbine during network unbalance," *IEEE Trans. Power Electron*., vol. 24, no. 11, pp. 2465–2474, Nov. 2009.
[30] G. Abad, M. A. Rodriguez, G. Iwanski, and J. Poza, "Direct power control of doubly-fed-induction generator-based wind turbines under unbalanced grid voltage," *IEEE Trans. Power Electron*., vol. 25, no. 2, pp. 442–452, Feb. 2010.
[31] M. S. Iyer and D. C. Wunsch II, "Dynamic reoptimization of a fed-batch fermentor using adaptive critic designs," *IEEE Trans. Neural Netw.*, vol. 12, no. 6, pp. 1433–1444, Nov. 2001.
[32] W. Liu, G. K. Venayagamoorthy, and D. C. Wunsch II, "A heuristic-dynamic-programming-based power system stabilizer for a turbogenerator in a single-machine power system," *IEEE Trans. Ind. Appl*., vol. 41, no. 5, pp. 1377–1385, Sep. 2005.
[33] G. K. Venayagamoorthy, R. G. Harley, and D. Wunsch, "Implementation of adaptive critic based neurocontrollers for turbogenerators in a multimachine power system," *IEEE Trans. Neural Netw.*, vol. 14, no. 5, pp. 1047–1064, Sep. 2003.
[34] N. Mohan, T. M. Undeland, and W. P. Robbins, *Power Electronics: Converters, Applications, and Design*, 3rd ed. New York: Wiley, Oct. 2002.
[35] A. Timbus, M. Liserre, R. Teodorescu, P. Rodriguez, and F. Blaabjerg, "Evaluation of current controllers for distributed power generation systems," *IEEE Trans. Power Electron*., vol. 24, no. 3, pp. 654–664, Mar. 2009.
[36] P. Giroux and G. Sybille. "Static synchronous compensator (STATCOM) used for midpoint voltage regulation on a 500kV transmission line," The MathWorks, Inc., Natick, MA, Jan. 2006.
[37] D. Zhi, L. Xu, and B. W. Williams, "Improved direct power control of grid-connected DC/AC converters," *IEEE Trans. Power Electron*., vol. 24, no. 5, pp. 1280–1292, May 2009.
[38] A. Sato and T. Noguchi, "Voltage-source PWM rectifier–inverter based on direct power control and its operation characteristics," *IEEE Trans. Power Electron*., vol. 26, no. 5, pp. 1559–1567, May 2011.
[39] E. Muljadi and C. P. Butterfield, "Wind farm power system model development," presented at the World Renewable Energy Congr. VIII, Denver, CO, Aug. 29–Sep. 3 2004.
[40] E. Muljadi, Y. Wan, C. P. Butterfield, and B. Parsons, "A study of a wind farm power system," presented at the 21st Amer. Soc. Mech. Eng. Wind Energy Symp., Reno, NV, Jan. 14–17, 2002.
[41] B. Shen, B. Mwinyiwiwa, Y. Zhang, and B. Ooi, "Sensorless maximum power point tracking of wind by DFIG using rotor position phase lock loop (PLL)," *IEEE Trans. Power Electron*., vol. 24, no. 4, pp. 942–951, Apr. 2009.
[42] P. Rodriguez, A. Timbus, R. Teodorescu, M. Liserre, and F. Blaabjerg, "Reactive power control for improving wind turbine system behavior under grid faults," *IEEE Trans. Power Electron*., vol. 24, no. 7, pp. 1798–1801, Jul. 2009.
[43] S. Li, T. A. Haskew, and R. Challoo, "Steady-state characteristic study for integration of DFIG wind turbines into transmission grid," *Int. J. Emerg. Electr. Power Syst*., vol. 10, no. 1, art. 7, Jan. 2009.
[44] B. G. Rawn, P. W. Lehn, and M. Maggiore, "Control methodology to mitigate the grid impact of wind turbines," *IEEE Trans. Energy Convers*., vol. 22, no. 2, pp. 431–438, Jun. 2007.
[45] X. Yuan, F. Wang, D. Boroyevich, Y. Li, and R. Burgos, "DC-link voltage control of a full power converter for wind generator operating in weak-grid systems," *IEEE Trans. Power Electron*., vol. 24, no. 9, pp. 2178–2192, Sep. 2009.

Shuhui Li (SM'06) received the B.S. and M.S. degrees in electrical engineering from Southwest Jiaotong University, Chengdu, China, in 1983 and 1988, respectively, and the Ph.D. degree in electrical engineering from Texas Tech University, Lubbock, in 1999.

From 1988 to 1995, he was with the School of Electrical Engineering, Southwest Jiaotong University, where he was involved in the research on modeling and simulation of large dynamic systems, dynamic process simulation of electrified railways, power electronics, power systems, and power system harmonics. From 1995 to 1999, he was involved in research on wind power, artificial neural networks, and applications of massive parallel processing. He joined as an Assistant Professor at Texas A&M University, Kingsville, in 1999, where he became an Associate Professor in 2003. He was with Oak Ridge National Laboratory for simulation system development on supercomputers in 2004 and 2006. He joined the University of Alabama, Tuscaloosa, as an Associate Professor in 2006. His current research interests include renewable energy systems, power electronics, power systems, electric machines and drives, flexible ac transmission system, intelligent control, microgrids, and distributed generation.

Timothy A. Haskew (M'86–SM'02) received the B.E.E., M.S., and Ph.D. degrees in electrical engineering from Auburn University, Auburn, AL, in 1987, 1988, and 1991, respectively.

He is currently a Professor of Electrical and Computer Engineering, University of Alabama, Tuscaloosa, where he serves as the Director of the Electromechanical Systems Laboratory and as the Electrical and Computer Engineering Graduate Program Director. Since 1991, he has been at the University of Alabama. He has authored or coauthored more than 50 refereed publications and two book chapters. His research interests include electromechanical systems, electric machinery, power electronics, and control systems.

Dr. Haskew is a member of the Power Electronics, Power and Energy, and Industry Applications societies of the IEEE. He has served as the Seminar Chair on the program committee for the IEEE Applied Power Electronics Conference.

Richard P. Swatloski received the B.S. and Ph.D. degrees in chemistry from the University of Alabama (UA), Tuscaloosa, in 2000 and 2005, respectively.

He has contributed to more than 50 peer-reviewed publications and multiple patents. His research has been presented more than 120 times at both national and international meetings, and is recognized as a leading Scientist in the field of ionic liquid chemistry. In 2006, he joined as a Licensing Associate and helped establish UA's Office for Technology Transfer. His current research interests include various aspects of intellectual property protection, management and licensing, agreement development, new business creation, and education.

Dr. Swatloski has received multiple awards and recognition, including the Kenneth G. Hancock Memorial Award for ionic liquid and green chemistry achievements. He is an active member in the Association for University Technology Managers (AUTM), and serves on the planning committee for AUTM's Annual Eastern Regional Meeting.

William Gathings, photograph and biography not available at the time of publication.